Materials & Design 223 (2022) 111249

Contents lists available at ScienceDirect

Materials & Design

journal homepage: www.elsevier.com/locate/matdes

Multiplexed detection of SARS-CoV-2 based on upconversion luminescence nanoprobe/MXene biosensing platform for COVID-19 point-of-care diagnostics

Menglin Song [a], Yingjing Ma [a], Lihua Li [a], Man-Chung Wong [a], Pui Wang [b], Jiangkun Chen [c], Honglin Chen [b], Feng Wang [c], Jianhua Hao [a,*]

[a] Department of Applied Physics, The Hong Kong Polytechnic University, Kowloon 999077, Hong Kong, China
[b] State Key Laboratory for Emerging Infectious Diseases, Department of Microbiology, Li Ka Shing Faculty of Medicine, The University of Hong Kong, Pokfulam 999077, Hong Kong, China
[c] Department of Materials Science and Engineering, City University of Hong Kong, Kowloon 999077, Hong Kong, China

HIGHLIGHTS

- 2D Nb_2CT_x nanosheets have the capability of quenching the fluorescence at wavelengths ranging from visible to near-infrared spectrum.
- Simple and label-free multiplexed RNA analysis strategy was developed.
- Upconversion luminescence nanoprobe/MXene biosensing platform enables rapid and sensitive detection of ORF and N gene of SARS-CoV-2 simultaneously.

GRAPHICAL ABSTRACT

We developed label-free multiplexed RNA analysis strategy based on the weakening of the FRET effect between different emission UCNPs and broad-spectrum quencher Nb_2CT_x to simultaneously detect ORF and N gene of SARS-CoV-2.

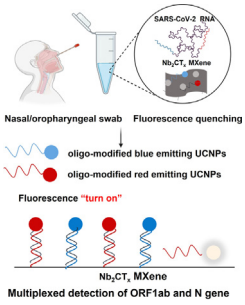

ARTICLE INFO

Article history:
Received 22 September 2022
Revised 6 October 2022
Accepted 9 October 2022
Available online 10 October 2022

Keywords:
Lanthanide-doped upconversion nanoparticles
Nb_2CT_x MXene
Multiplexed detection
SARS-CoV-2

ABSTRACT

Multiplexed detection is essential in biomedical sciences since it is more efficient and accurate than single-analyte detection. For an accurate early diagnosis of COVID-19, a multiplexed detection strategy is required to avoid false negatives with the existing gold standard assay. Nb_2CT_x nanosheets were found to efficiently quench the fluorescence emission of lanthanide-doped upconversion luminescence nanoparticles at wavelengths ranging from visible to near-infrared spectrum. Using this broad-spectrum quencher, we developed a label-free FRET-based biosensor for rapid and accurate detection of SARS-CoV-2 RNA. To target ORF and N genes, two types of oligo-modified lanthanide-doped upconversion nanoparticles can be used simultaneously to identify-two sites in one assay via upconversion fluorescence enhancement intensity measurement with detection limits of 15 pM and 914 pM, respectively. Moreover, with multisite cross-validation, this multiplexed and sensitive biosensor is capable of simultaneous and multicolor analysis of two gene fragments of SARS-CoV-2 Omicron variant within minutes in a single homogeneous solution, which significantly improves the detection efficiency. The diagnosis

* Corresponding author.
E-mail address: jh.hao@polyu.edu.hk (J. Hao).

https://doi.org/10.1016/j.matdes.2022.111249

result *via* our assay is consistent with the PCR result, demonstrating its application in the rapid and accurate screening of multiple genes of SARS-CoV-2 and other infectious diseases.

1. Introduction

The outbreak of novel coronavirus disease (COVID-19) caused by severe acute respiratory syndrome coronavirus 2 (SARS-CoV-2) is highly transmissible to humans and in some cases may even be fatal, which has triggered a global public health crisis [1]. Lung computed tomography (CT) scanning of patients based on specific imaging features is one of diagnostic method of COVID-19, but the accuracy of 76.4 % and untimely diagnosis limit its further implement [2]. Further, antibody serology assays can only detect antibodies within 1–2 weeks after disease onset, making early diagnosis difficult [3]. Rapid antigen tests have shown promise as means of obtaining results in a shorter period of time and requiring less sample preparation. However, its sensitivity is criticized by the majority of users, resulting in challenges for early and accurate diagnosis [4]. Current nucleic acid amplification testing (NAAT) such as reverse transcription-polymerase chain reaction (RT-PCR) is often used to detect the nucleic acids extracted from the SARS-CoV-2 specimens owing to optimized sensitivity, specificity, and ease of quantitative analysis [5]. However, the testing process is hindered by the long turnaround times, expensive laboratory equipment and trained personnel. As a gold standard, qPCR is plagued by the problem of false negatives. According to the new Coronavirus pneumonia diagnosis and treatment plan of the National Health Commission of China, up to 20–67 % of patients test positive only after multiple repeated tests [6,7].

In order to diagnose SARS-CoV-2 accurately and rapidly, it is highly anticipated to develop point-of-care multiplexed detection strategies for the cross-validation of multiple characteristic-related biomarkers. The U.S. Center for Disease Control and Prevention (CDC) provides examples of gene selection and multi-component testing methods [8]. For each patient's sample, three qPCR reactions were performed sequentially, in accordance with the guidelines set forth by the World Health Organization (WHO) [9]. Additionally, a variety of biosensors have been developed for multi-component detection, including electrochemical biosensors [10], colorimetric biosensors [11] and loop-mediated isothermal amplification (LAMP) using clustered regularly interspaced short palindromic repeats (CRISPER) [12]. Despite their success, the results of these biosensors were hampered by the undesired aggregation [13] and lengthy turnaround time [14]. Therefore, it became urgently necessary to develop rapid, sensitive, and specific diagnostic tools for multiplexed detection of the virus and its mutated forms.

Förster resonance energy transfer (FRET) has been widely used in biomedical and clinical applications to access molecular scale information [15]. Such a phenomenon occurs when the emission spectrum of the donor fluorophore overlaps with the absorption spectrum of the acceptor fluorophore between two proximal fluorophores [16]. According to *E1*, the efficiency of this transfer depends on the distance between the two fluorophores. Inverse sixth power dependence makes FRET measurements extremely sensitive to even small changes in distance. Based on the intrinsic properties, various FRET-based biosensors have been designed for virus detection [17]. Among these assays, the bio-receptors interact with the biomarkers of interest and induce a change in the luminescence intensity. Hence, the chemical and physical properties of the transducer/fluorophore are vital in the detection. Most organic dyes are subject to photobleaching, whereas inorganic quantum dots are prone to blinking. A further limitation is that their excitation wavelengths are typically in the UV–vis range, which severely limits the sensing sensitivity due to fluorescent background derived from biomolecules, as well as internal filtering effects due to absorption by other species [18,19]. Fortunately, these disadvantages might be mitigated by utilizing lanthanide (Ln^{3+})-based upconversion nanoparticles (UCNPs) as fluorescence donors. UCNPs can absorb two or more low-energy photons and produce luminescence at a short wavelength than the excitation wavelength. The inner 4f-4f orbital electronic transitions, which are protected by the full 5s and 5p orbitals, are responsible for the upconversion fluorescence. Besides, the long-lived emission of Ln^{3+}-based probes would improve lifetime measuring accuracy and allows for time-resolved detection or even multiplexed sensing by using various Ln^{3+} combinations. Because of their excellent chemical and photochemical stability, large anti-Stokes shift, low toxicity, lack of photobleaching, blinking and autofluorescence, UCNPs is well suited for biosensing detection.

Niobium carbide (Nb_2C) MXene is a new emerging 2D material and its unique physical and chemical properties of Nb_2CT_x are very versatile and termination-dependent, making it desirable for various application including electrochemical biosensors [20], energy storage [21] and theranostics [22]. Its large surface area facilitates multiple-donor–single-acceptor configurations and broad absorption endows it high luminescence quenching ability, which makes it favorable for developing the FRET-based biosensor applicable to multiplexed detection [23,24].

Considering these merits, here we develop a novel, simple and label-free FRET based biosensor for multiplexed detection of SARS-CoV-2 RNA. The test is relied on the Förster distance changes between the donors of oligo-modified different emission UCNPs and the acceptor of Nb_2CT_x, in which simultaneous detections of ORF1ab gene and N gene were performed, showing excellent selectivity and sensitivity. We adopted this simple "mix and detect" strategy for multiplex detection based on the following three considerations: (i) the analysis of two genes in one tube may increase the detection sensitivity, resulting in accumulation of detection signals, (ii) analyzing two genes simultaneously may improve detection efficiency because one positive signal of the two genes indicates SARS-CoV-2 infection, (iii) screening of COVID-19 can be more effective with the rapidity and simplicity of the detection workflow. Furthermore, with the capability of multisite cross-validation, the biosensor had been evaluated using SARS-CoV-2 variant (B.1.1.529/Omicron) clinical samples, which successfully distinguished the ORF and N gene. Positive or negative result of viral gene testing can be obtained within 5 min, which is fully in agreement with the PCR results. Thus, our simple and label-free multiplexed detection strategy enables on-site rapid and sensitive detection of multiple gene simultaneously and it can also be extended to the bio-detections of other nucleic acid and biomarkers.

2. Materials and methods

2.1. Materials

Nb_2AlC (>99 %) was purchased from Laizhou Kai Ceramic material Co., LTD. Lanthanide (Ln) acetates (99.9 %), including thulium (Tm), erbium (Er), gadolinium (Gd), and ytterbium (Yb) were dis-

solved in D.I. water to form 0.2 M aqueous solution. 1-octadecene (1-ODE, 90 %, technical grade), Oleic acid (OA, 90 %, technical grade), cyclohexane (ACS grade, 99 %), ethanol (99.9 %), sodium hydroxide (NaOH, ACS grade, 97 %), methanol (99.9 %), concentrated hydrochloric acid (HCl, 37 %), phosphate buffered saline (PBS, Bio Performance, pH = 7.4) were purchased from Sigma-Aldrich. Ultrapure water (molecular biology grade) is used in all experiments involving DNA oligonucleotides (oligos). DNA oligos were purchased from Integrated DNA Technologies, Inc. All these chemicals were used as received without further purification.

2.2. Synthesis of few layers Nb_2CT_x MXene

Nb_2CT_x MXene is typically synthesized by selectively etching Nb_2AlC with 5 M LiF/6 M HCl solution for 48 h at room temperature. Upon completion of the etching process (complete removal of Al elements), it is necessary to wash the product three times to remove the residual acid and salt. The multi-layered Nb_2CT_x MXene can be collected when the pH of the solution reaches 6. In the delamination step, TMAOH was used as an intercalant. 12 mL 25 % TMAOH was reacted with multi-layered MXene (20 mg) for 12 h. After the reaction, the suspension was washed and collected by centrifugation to obtain TMA-intercalated Nb_2CT_x. The sediment was dispersed in 2 mL distilled water, and the multi-layered MXene was further delaminated for 10 min by sonication, and then the solution was centrifuged to collect the few-layered Nb_2CT_x. To alleviate its oxidation, the obtained MXene was dried in vacuum.

2.3. Synthesis of blue-emitting $NaGdF_4$:Yb/Tm UCNPs

In a typical coprecipitation synthesis, 0.008 mmol of thulium (III) acetate hydrate, 0.072 mmol of ytterbium (III) acetate, 0.32 mmol of gadolinium (III) acetate hydrate 4 mL OA and 6 mL ODE were added to a 50 mL three-necked flask under magnetic stirring at room temperature. The mixture was heated to 100 ℃ for 30 min to remove the water followed by 150 ℃ for 1 h to form the lanthanide-oleate coordination complexes. After that, removed the heating mantle and cooled the mixture to room temperature under magnetic stirring. To trigger the nucleation and growth of the $NaGdF_4$ nanocrystals, 1 mmol NaOH-methanol stock solution and 1.32 mmol NH_4F-methanol stock solution were then mixed by vortexing for 10 s to prevent NaF generated from sticking to the wall of the centrifuge tube and immediately injected it into the reaction mixture. Next, the temperature was raised to 50 ℃ and keep it for 1 h under magnetic stirring to promote the crystal growth. Connect the flask to a dual vacuum/gas manifold and degas for 10 min, and then raise the temperature to 290 ℃, and keep it for 1.5 h under the protection of argon. After the synthesis was finished, let the reaction mixture to cool to ambient temperature while stirring. The crude UCNPs was transferred into a 15 mL centrifuge tube, rinse the flask with 5 mL ethanol, and combine it into the centrifuge tube. The product was centrifuged at 6000 r.p.m. (∼3500 g) at room temperature for 3 min, and then purified using cyclohexane and ethanol. Finally, the UCNPs were dispersed in 4 mL fresh cyclohexane for further use.

2.4. Synthesis of red emitting-$NaErF_4$:Tm UCNPs

0.398 mmol of erbium (III) acetate hydrate, 0.002 mmol of thulium (III) acetate, 4 mL OA, and 6 mL ODE were introduced to a 50 mL three-necked flask with magnetic stirring at room temperature. The mixture was heated to 100 °C for 30 min to remove water before being heated to 150 °C for 1 h to create the lanthanide-oleate coordination complexes. The heating mantle was then removed, and the fluid was cooled to room temperature using magnetic stirring. To initiate the nucleation and growth of the $NaErF_4$ nanocrystals, 1 mmol NaOH-methanol stock solution and 1.32 mmol NH_4F-methanol stock solution were vortexed for 10 s to prevent the NaF produced from clinging to the wall of the centrifuge tube and then introduced into the reaction mixture. The temperature was then increased to 50 °C and maintained for 1 h under magnetic stirring to promote crystal formation. Connect the flask to a dual vacuum/gas manifold and degas for 10 min before raising the temperature to 290 °C and keeping it there for 1.5 h under argon protection. After the synthesis was finished, the liquid was progressively cooled to room temperature while being stirred. The crude UCNPs were put into a 15 mL centrifuge tube, and the flask was rinsed with 5 mL ethanol before being combined into the centrifuge tube. The product was centrifuged at 6000 r.p.m. (3500g) for 3 mins at room temperature before being purified with cyclohexane and ethanol. Finally, the UCNPs were dispersed in 4 mL of fresh cyclohexane for further use.

2.5. Synthesis of ligand-free UCNPs

The UCNPs dissolved in cyclohexane were centrifuged and redispersed in dilute hydrochloric acid at pH ∼ 4. Then, the mixture was treated with sonication for 30 mins, followed by centrifugation at 14,000 rpm for 30 min and discard the supernatant. Next, repeat these washing steps until the brown color disappears. Then, wash it with deionized water to remove the excess acid. Finally, the obtained ligand-free UCNPs were dispersed in deionized water.

2.6. UCNPs modification with poly C10-complementary oligo

The ligand-free UCNPs ($NaGdF_4$:Yb/Tm; $NaErF_4$:Tm) were dispersed in 600 μL D.I. water, and the suspended UCNPs mixture was slowly added to an aqueous solution (300 μL) containing different types of C10-complementary DNA under the sonication, followed by the addition of 20 μL of 10 × TB-Na^+ buffer (890 mM tris base, 890 mM bonic acid, 1 M NaCl, pH ∼ 8) to the mixture per hour for a total volume of 100 μL, making the nanocomposites dispersed in 1 × TB-Na^+buffer. After incubation for overnight, the solution was purified with a 0.22 μm filter to remove large aggregates. Finally, free DNA in the supernatant were discarded by centrifugation to obtain DNA-modified UCNPs. The prepared DNA-modified UCNPs can be characterized by UV–vis spectroscopy.

2.7. FRET efficiency calculation

Nonradiative energy transfers are dependent on spectral overlap and intermolecular distance according to Theodor Forster's quantitative theory. According to Forster, energy transfer rate is calculated as an integral of spectral overlap. The simplified equation for FRET efficiency is as follows:

$$E = \frac{1}{1 + \left(\frac{R}{R_0}\right)^6} \tag{1}$$

when the transfer efficiency is 50 %, a fluorescent distance between donors and acceptors is defined as R_0. Where R is the distance between donors and acceptors. There is an inverse relationship between energy transfer efficiency E and distance between donors and acceptors. The transfer rate is about to reach its maximum ($<R_0$) with a decreasing distance R. Forster showed that R_0 could be calculated using overlap integrals, which is in accordance with previous experiments. Thus, the molecular distance between donors and acceptors can be determined by calculating E and R_0.

2.8. PL response for nucleic detection

To verify the DNA probe detection, 1×10^{-9} M of each *P*1 and *P*2 modified probe were hybridized with different concentration of T1 and T2 (target DNA or SARS-CoV-2 RNA) in 494 μL of phosphate buffer (0.1 M, pH 7.4) respectively and followed by adding the Nb_2CT_x MXene aqueous with the final concentration of 200 μg mL^{-1}. Fluorescence spectra were monitored by the FLS920P Edinburgh Instrument at room temperature. From UCL spectra, the fluorescence intensity enhancement efficiency (η_x) can be calculated by the *E2*.

$$\eta_x\% = \frac{I_x - I_0}{I_0} \times 100\% \quad (2)$$

2.9. Virus and cell line

A strain of B.1.1.529/Omicron (GeneBank: OM212472) has been isolated from the respiratory tract of COVID-19 patients at The University of Hong Kong. All experiments involving live SARS-CoV-2 were performed in accordance with approved operating procedures. A DMEM medium containing 10 % FBS, 2 mM L-glutamine, and 100 U/mL/mL penicillin was used to culture Vero-E6-TMPRSS2 cells. The cells were incubated at 37 °C in a CO_2 atmosphere at 5 %. The sequences of all variants of this virus were determined through nanopore sequencing after virus cultures were obtained. A commercial RT-PCR kit (Novel Coronavirus (2019-nCoV) Dual Probes RT-PCR Kit; Beyotime, China) and a detection system (Applied Biosystems QuantStudio 5 Real-Time PCR System, Thermo Fisher Scientific, USA) were used to amplify extracted RNA for clinical diagnosis. RT-PCR results with a Ct value, 35 were considered positive.

3. Result and discussion

3.1. Multiplexed detection strategy

A simple, label-free and sensitive MXene-integrated biosensor was designed for multiplexed detection of SARS-CoV-2 RNA sequences. The design strategy is shown in Fig. 1. During the process, different emitting UCNPs labeled with complementary oligonucleotides, serve as fluorescent probes, were fixed on MXene nanosheets due to noncovalent binding. Nb_2CT_x nanosheets quenched the fluorescence of UCNPs under the effect of FRET. The complementary oligo-labeled UCNPs hybridized with the RNA target to form double-stranded structure. Thus, nucleobases are buried between the densely negatively charged helical phosphate backbones which has strong repulsion with negatively charged Nb_2CT_x MXene, resulting in different emitting oligo-modified UCNPs desorbed from MXene and fluorescence signals turn on. It is worth mentioning that the long RNA sequences are prone to undergo unwanted aggregation and entanglement. Dual fluorescence probes were employed to indirectly increase the hybridization site of the target, thus enhancing the sensitivity and improving the detection efficiency *via* multisite cross-validation.

3.2. Synthesis and characterization of few-layer Nb_2CT_x and blue/red-emitting UCNPs

We synthesized high-quality 2D few-layer Nb_2CT_x NSs using a facile and scalable two-step method involving acid etching and intercalation. Currently, a top-down approach is widely employed for fabricating MXene by selective etching from their MAX phases. Owing to high chemical activity of the metallic Nb-C bonds, Nb_2CT_x MXene can be obtained at room temperature by eliminating weaker Nb-Al bonds from Nb_2AlC powder in an aqueous 50 % hydrofluoric acid (HF). In Fig. S1, the (002) peak of Nb_2C MXene is shifted to the lower 2θ position, which signals expanded interlayer spacing, demonstrating the successful synthesis of Nb_2CT_x nanosheets (NSs). To obtain the few-layer nanosheets, tetrabutylammonium hydroxide (TBAOH) was used to exfoliate 2D layered Nb_2CT_x. Protons (H^+) exchange with bulky tetrabutylammonium ions (TBA^+) which results in the material swelling and delamination. Fig. 2A illustrates typical 2D morphology of the exfoliated Nb_2C NSs, with transparent features evidence of ultrathin properties of the MXenes. As shown in Fig. 2B, selected area electron diffraction (SAED) pattern demonstrates the hexagonal symmetry

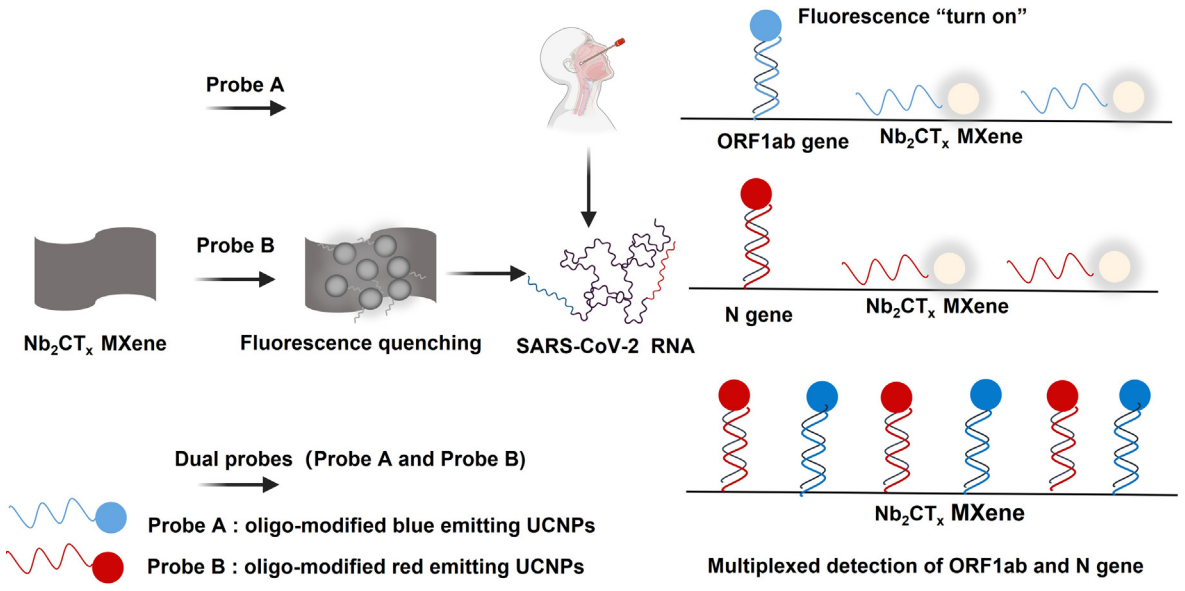

Fig. 1. The schematic illustration of the rapid multiplexed detection of SARS-CoV-2 RNA with enhanced sensitivity and detection efficiency based on a dual-upconversion emission/MXene integrated nanoplatform.

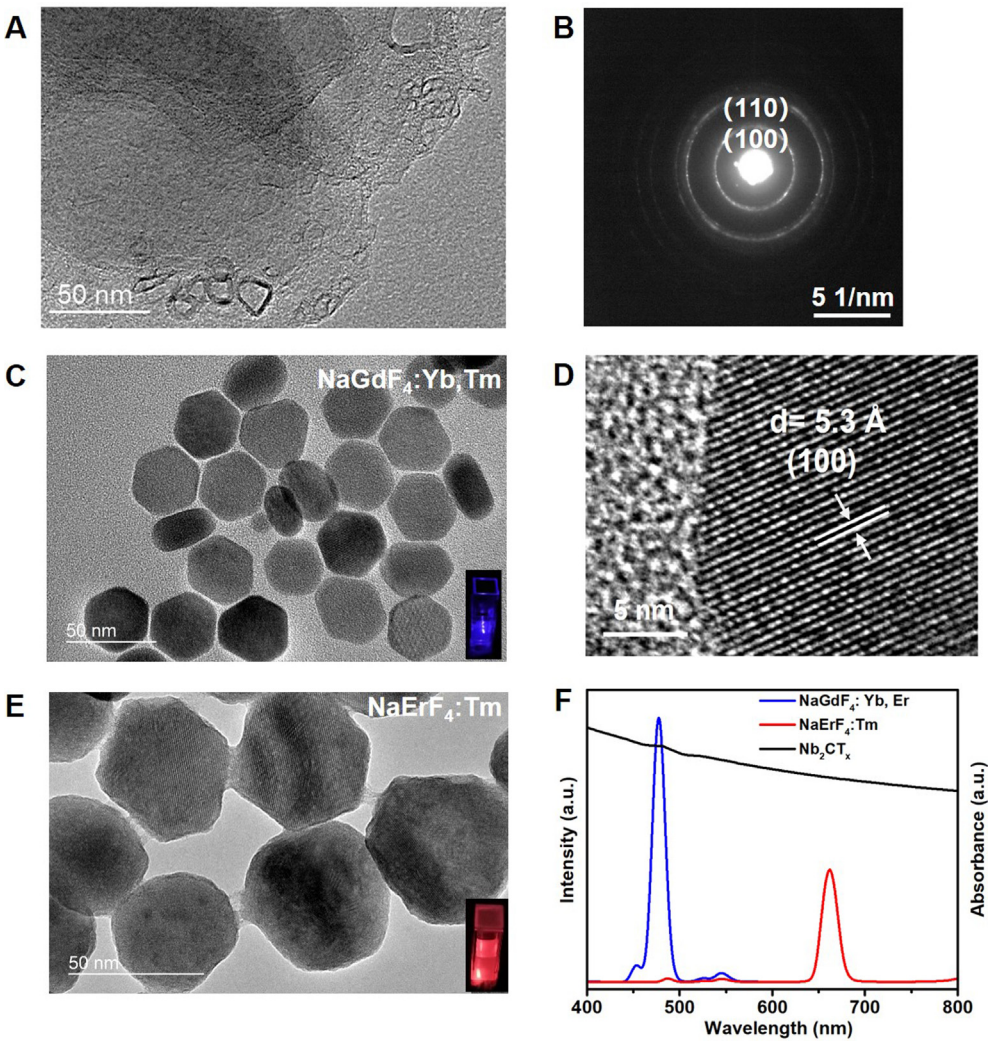

Fig. 2. (A). TEM of few-layer Nb_2CT_x MXene. (B). SAED pattern of few-layer Nb_2CT_x nanosheets; (C). TEM and (D). HR-TEM images of $NaGdF_4$:Yb,Tm. (E). TEM image of $NaErF_4$, Tm UCNPs. (F). UV–vis absorption of Nb_2CT_x overlaps the blue-emitting and red-emitting UCNPs. The inset images in (C) and (E) are blue and red emission of $NaGdF_4$:Yb,Tm and $NaErF_4$,Tm UCNPs. (For interpretation of the references to color in this figure legend, the reader is referred to the web version of this article.)

structure of Nb_2C NSs. The blue-emitting $NaGdF_4$:Yb, Tm is well dispersed in the cyclohexane and displays exceptional crystallinity with a lattice spacing of 5.1 nm, which is indexed to the (100) plane of a hexagonal $NaGdF_4$ crystal, as demonstrated in high resolution transmission electron microscopy (HR-TEM) images (Fig. 2D). Fig. 2E illustrates the mono-dispersibility of oleate-capped red emitting UCNPs ($NaErF_4$:Tm) in cyclohexane, which were spherical in form and averaged 48 nm in size. The $NaErF_4$:Tm UCNPs exhibited outstanding crystallinity with a lattice spacing of 5.4 Å, corresponding to the (100) plane of a hexagonal $NaGdF_4$ crystal (Fig. S2). Considering its good biocompatibility, large surface area, abundance of terminations (—O—/OH—) and broad absorption across UV–vis-NIR spectrum, Nb_2CT_x is well suited for an outstanding substrate as well as a fluorescence quencher in a FRET-based biosensing system, allowing multiple-donor–single-acceptor configurations to be realized in a multiplexed detection. Fig. S3 demonstrates the absorption spectrum of different concentration of Nb_2CT_x and the absorption enhanced as the increment of the concentration of MXene. Additionally, as shown in Fig. 2F the blue and red emissions of two probes are well overlapped with the absorption of Nb_2CT_x NSs, and the quenching efficiency was calculated to be 80.82 % and 69.29 % (Figs. S4 and S5), offering great potential for fluorescence recovery and providing great possibility for ultrasensitive multiplexed detection.

3.3. Ultrasensitive detection of short oligonucleotide fragments

Based on aforementioned results and well-established fact of DNA-MXene interaction, we designed an MXene-integrated biosensor for multiplexed real-time SARS-CoV-2 RNA fragments detection. The fluorescent signal of UCNPs is turned on and increases with the concentration of targets. The spectral overlap between the blue/red emitting UCNPs and the absorption properties of Nb_2CT_x indicates the FRET efficiency of this integrated biosensor. Fig. 3**A** shows the upconversion spectra of short ORF1ab-target detection using the FRET-based integrated assay. When the UCNPs-P1 contact with the Nb_2CT_x MXene, the emission intensity drops owing to the FRET effect between UCNP and Nb_2CT_x MXene. However, with increment of the amount of target, the intensity of UCNPs at 481 nm enhanced accordingly. The oligo modified UCNPs were specifically bound with the complementary oligo target via hybridization, resulting in weakened noncovalent

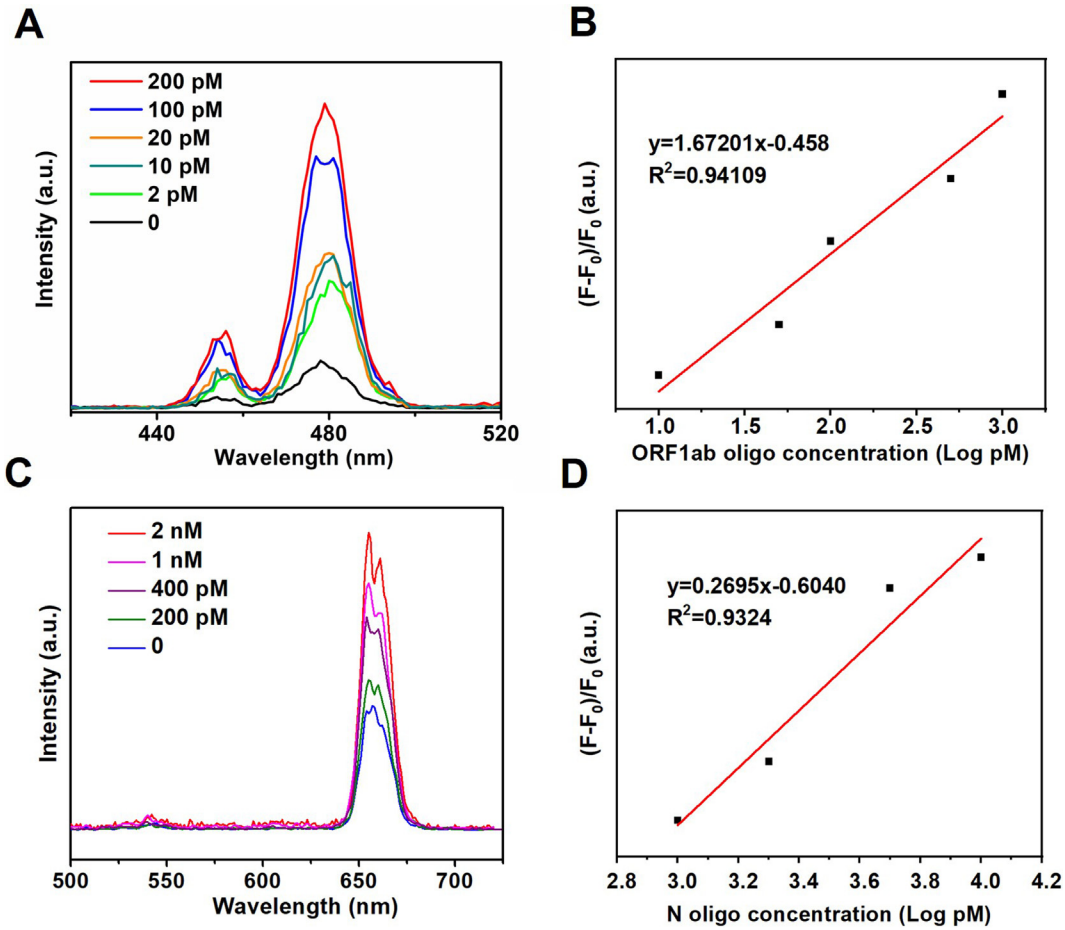

Fig. 3. (A and B) UC emission spectra of the Nb_2CT_x/blue-emitting UCNP assay in the presence of different concentrations of short ORF1ab target. (C and D) UC emission spectra of the Nb_2CT_x/red-emitting UCNP assay in the presence of different concentrations of short *N*-gene target. (For interpretation of the references to color in this figure legend, the reader is referred to the web version of this article.)

binding ability. Therefore, the double strands structure will be detached from the MXene, which in turn will result in a longer Förster distance, thus increasing the luminescence intensity of UCNPs. The limit of detection (LOD) was determined to be 12 pM for ORF detection using the control signal plus three times standard derivation (Fig. 3**B**). The upconversion spectra of *N*-target detection utilizing the MXene-based integrated assay are shown in Fig. 3**C**. A similar phenomenon also occurs between UCNP-P2 and Nb_2CT_x, the intensity of UCNPs at 660 nm enhanced with increment concentration of *N*-target oligo, the UCNPs-probe specifically bound with the short gene via hybridization, resulting in weakened noncovalent binding ability. As the concentration of N target oligonucleotide increased, the recovered fluorescence was enhanced accordingly. As a result, the LOD was calculated to be 95 pM. (Fig. 3**D**).

3.4. Multiplexed simultaneous detection of long DNA fragments

We have successfully demonstrated the ultrasensitive detection of short ORF1ab and N oligo fragments using our UCNPs/MXene integrated biosensors. However, the clinical viral samples containing long gene sequences undergo unwanted aggregation and entanglement, increasing the steric hindrance, thus resulting in low sensitivity of the proposed biosensor (Fig. 4**A**). To compensate for this risk of reduced sensitivity and enhance the detection efficiency, we developed a label-free approach for multiplexed upconversion fluorescence detection of long DNA fragment. The long DNA sequences are shown in Table S1. As shown in Fig. 4**B and 4C**, two oligo modified probes with different upconversion emission can be mixed and quantified in one single assay. It is observed that blue and red emission intensities increase simultaneously with the presence of long DNA fragments. Calibration curves were formed in the simultaneous detection protocol using luminescence intensity enhancement as a function of the varying concentrations of long DNA targets (ORF1ab and N gene), enabling rapid and sensitive detection of ORF1ab and N gene (Fig. S6). The LOD were determined to be 15 pM and 914 pM for long simulated ORF1ab and N gene, which is slightly higher than that for short oligo detection owing to unwanted aggregation and entanglement of long gene sequence. To evaluate the analytical specificity of our proposed assay, a cross-reaction analysis was executed. The obtained results in Fig. 4**D and 4E** show that the assay is capable of distinguishing SARS-CoV-2, SARS-CoV and bat-SL-CoVZC45. The upconversion intensity enhancement at 481 nm were 18.44 % for SARS-CoV, 30.54 % for bat-SL-CoVZC45 and 82.81 % for SARS-CoV-2, respectively. The test shows excellent specificity, thus it can be used for evaluating clinical samples.

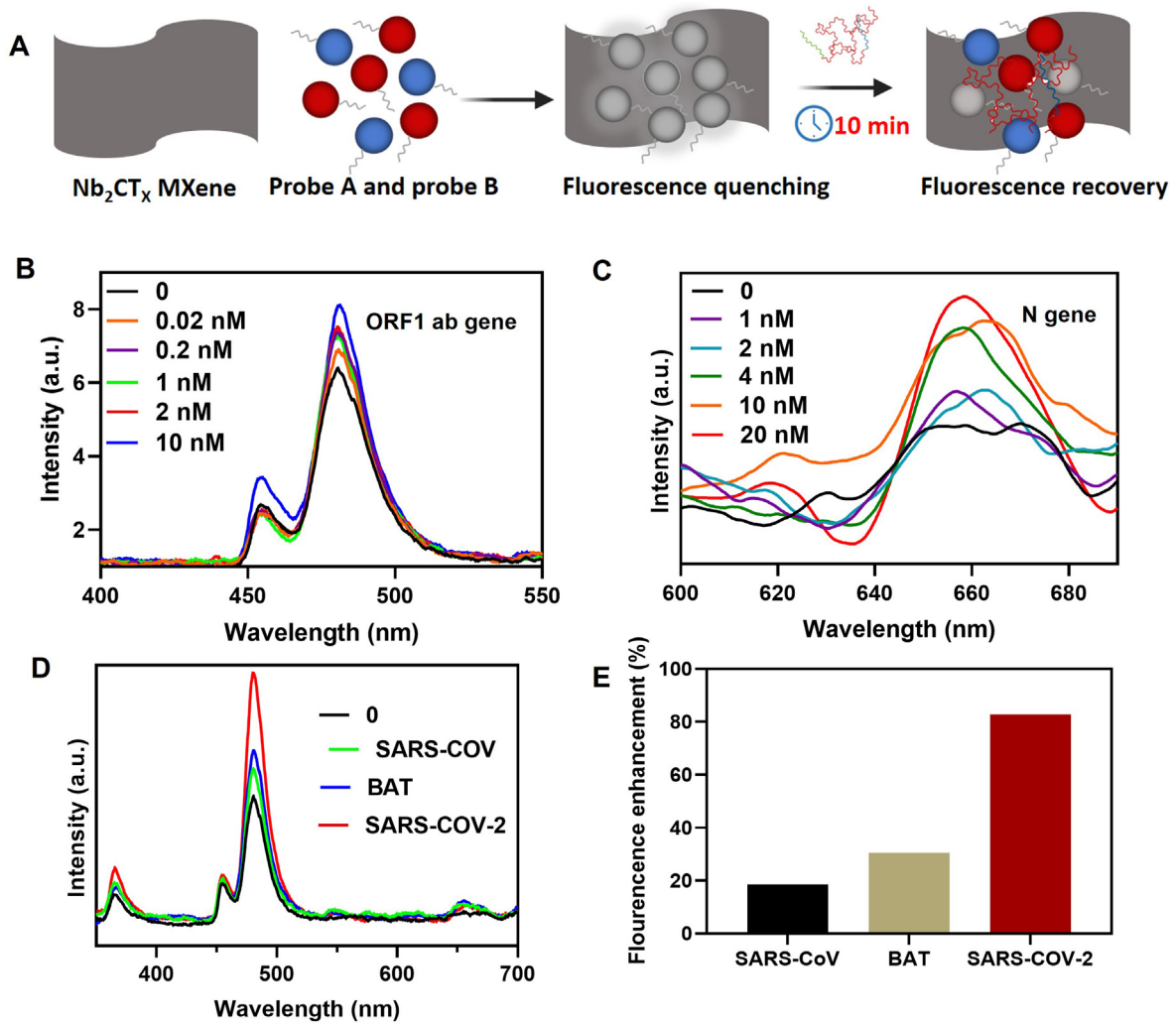

Fig. 4. (A) The scheme of detection of long simulated target using dual emission UCNPs/MXene integrated biosensor. Photoluminescence spectra at different emission bands of the proposed biosensor for simultaneous multiplexed detection of (B) ORF-1ab and (C) *N*-target. (D) PL intensity recovery comparison for RNA-targeted regions among three highly homologous coronavirus. (E) The specificity analysis of the using dual emission UCNPs /MXene integrated biosensor.

3.5. Detection of SARS-CoV-2 Omicron (B.1.1529) variant samples

To demonstrate the readiness of the dual emission UCNPs/MXene integrated biosensor for rapid multiplexed detection of COVID-19, we applied it to the clinic diagnosis test. A positive control was conducted by using RT-PCR to detect the ORF gene of viral samples with defined quantities before testing clinic samples. Virus-free kit buffer and lysis buffer were used as negative controls. The cycle threshold (Ct) values of kit buffer and lysis buffer by RT-PCR were 34.989 ± 1.651 and 36.155 ± 2.556, whereas for viral samples with quantities of 0.5 μL, and 1 μL, each Ct values were 25.181 ± 0.381 and 22.955 ± 2.315, respectively (Fig. 5**A**). Based on clinical reports of diagnosing COVID-19 patients with ORF genes, the Ct values of positive RT-PCR results are less than 35. Having determined the Ct values of the specific quantities of viral samples, we then mixed each viral sample with a mixture containing Nb_2CT_x and oligo modified UCNPs. It is encouraging to note that the fluorescence intensities at 481 and 658 nm would have recovered after 5 min of hybridization, indicating the presence of the ORF gene and N gene of SARS-CoV-2 (Fig. 5**B and C**). Fig. 5**D** illustrates the fluorescence enhancement at 481 nm and 658 nm of 20.04 %, 20.02 % when 0.5 μL of virus sample was added. For the 1 μL virus sample, the fluorescence enhancements were 24.18 % (481 nm) and 17.62 % (658 nm), respectively. A significant increase in intensity of the viral sample groups compared with the control group is associated with the presence of target RNA that activates the "Turn-on" mechanism of our assay. These results demonstrate that our assay realize multiplexed detection of SARS-CoV-2 ORF and N gene and enables high-sensitivity screening of positive and negative samples through PL spectrum. As a result, the diagnosis result via our assay in good agreement with the RT-PCR results, indicating that with a significantly shorter turnaround time of 5 min, our assay is capable of reliably screening the SARS-CoV-2 Omicron variants (B.1.1.529). This effective and rapid method thus provides an efficient alternative to commercial RT-PCR. The fast sample-to-answer time, simplicity of workflow, high sensitivity and multisite cross-validation of this test make it a possible replacement for the current rapid antigen tests at multiple point-of-care scenarios.

A

Sample	Kit Buffer	Lysis Buffer	Viral sample (Omicron/B.1.1.529)	
			0.5 μL	1 μL
Ct-value	34.989 ± 1.651	36.155 ± 2.556	25.181 ± 0.381	22.955 ± 2.315

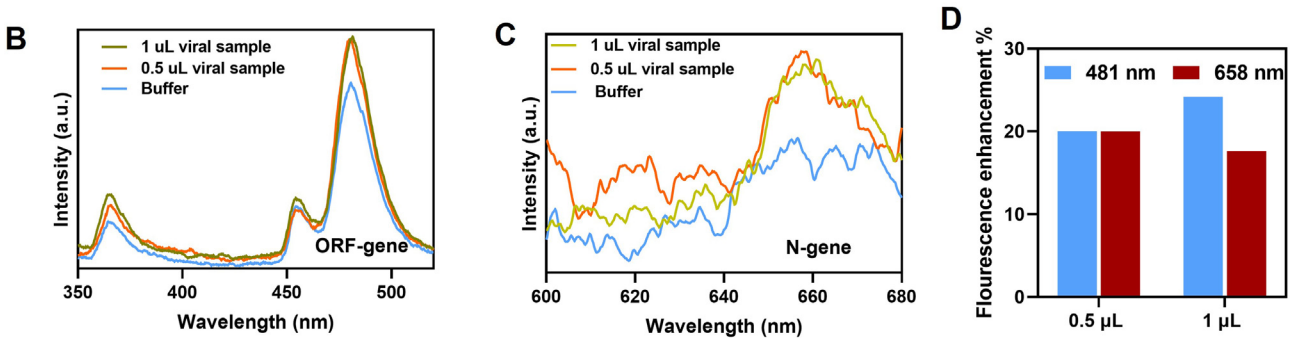

Fig. 5. (A) RT-qPCR results of ORF-gene in different volume viral samples (different amount viral samples serve as positive control groups, while the kit buffer and lysis buffer without virus and serves as negative control groups). (B) Blue emission and (C) red emission of UCNPs/MXene integrated biosensor when adding viral sample (0.5 μL and 1 μL of SARS-CoV-2 Omicron/B.1.1529 stock solution extracted from cells, sample to answer time: 5 min). (D) Peak intensities enhancement of the Nb_2CT_x/UCNP integrated biosensor after probing different quantities of viral samples, corresponding to (B) and (C). (For interpretation of the references to color in this figure legend, the reader is referred to the web version of this article.)

4. Conclusion

Herein, we developed label-free multiplexed RNA analysis strategy based on the weakening of the FRET effect between different emission UCNPs and broad-spectrum quencher Nb_2CT_x to simultaneously detect two specific RNA gene sites of SARS-CoV-2. By measuring the upconversion fluorescence enhancement intensity, rapid and sensitive detection of ORF and N gene can be achieved in one single assay with limits of 15 pM and 914 pM, respectively. Additionally, this multiplexed and sensitive biosensor can be used to analyze two RNA fragments of SARS-CoV-2 Omicron variant for COVID-19 point-of-care diagnostics. The results obtained with the test system were in agreement with those tested by PCR, showing its great potential for rapid detection of multiple genes related to SARS-CoV-2 and other infectious diseases.

Data availability

Data will be made available on request.

Declaration of Competing Interest

The authors declare that they have no known competing financial interests or personal relationships that could have appeared to influence the work reported in this paper.

Acknowledgements

The research was supported by the grants from the Research Grants Council of the Hong Kong Special Administrative Region, China (Project No. CRF No. PolyU C5110-20G and GRF 15301020).

Data availability.

Data will be made available on request.

Author Contributions.

All authors have given approval to the final version of the manuscript. M.S. and J.H. conceived the method and planned the experiments. M.S., Y.M., L. L. and M.C.W. performed the experiments. P.W. and H.C. provided the SARS-CoV-2 samples. J. C. and F. W. assisted with PL measurements. M.S., J.H. and L. L. analyzed the data. J.H. supervised projects. M.S. and J.H. wrote the manuscript.

Appendix A. Supplementary material

Supplementary data to this article can be found online at https://doi.org/10.1016/j.matdes.2022.111249.

References

[1] H. Harapan, N. Itoh, A. Yufika, W. Winardi, S. Keam, H. Te, D. Megawati, Z. Hayati, A.L. Wagner, M. Mudatsir, Coronavirus disease 2019 (COVID-19): a literature review, J. Infect. Public Health 13 (5) (2020) 667–673.
[2] W. Guan, Z. Ni, Y. Hu, W. Liang, C. Ou, J. He, L. Liu, H. Shan, C. Lei, D.S. Hui, Clinical characteristics of coronavirus disease 2019 in China, NEJM 382 (18) (2020) 1708–1720.
[3] C. Sheridan, Fast, portable tests come online to curb coronavirus pandemic, Nat. Biotechnol. 38 (5) (2020) 515–518.
[4] A. Scohy, A. Anantharajah, M. Bodéus, B. Kabamba-Mukadi, A. Verroken, H. Rodriguez-Villalobos, Low performance of rapid antigen detection test as frontline testing for COVID-19 diagnosis, J. Clin. Virol. 129 (2020) 104455.
[5] T. Nolan, R.E. Hands, S.A. Bustin, Quantification of mRNA using real-time RT-PCR, Nat. Protoc. 1 (3) (2006) 1559–1582.
[6] W.J. Wiersinga, A. Rhodes, A.C. Cheng, S.J. Peacock, H.C. Prescott, Pathophysiology, transmission, diagnosis, and treatment of coronavirus disease 2019 (COVID-19): a review, JAMA 324 (8) (2020) 782–793.
[7] National Health Commission of the People's Republic of China and Traditional Chinese Medicine of the People's Republic of China (2020) Guidelines for the Diagnosis and Treatment of Coronavirus Disease, 2019 (Trial Version 7).
[8] CDC, CDC 2019-Novel coronavirus (2019-nCoV) real-time RT-PCR diagnostic panel, Centers for Disease Control and Prevention, 2020.
[9] F. CDC, CDC 2019-nCoV real-time RT-PCR diagnostic panel, FACT SHEET FOR HEALTHCARE PROVIDERS.[Online] June 12, 2020. <https://www. fda. gov/media/134920/download>.
[10] R.M. Torrente-Rodriguez, H. Lukas, J. Tu, J. Min, Y. Yang, C. Xu, H.B. Rossiter, W. Gao, SARS-CoV-2 RapidPlex: a graphene-based multiplexed telemedicine platform for rapid and low-cost COVID-19 diagnosis and monitoring, Matter 3 (6) (2020) 1981–1998.
[11] R. He, H. Liu, T. Fang, Y. Niu, H. Zhang, F. Han, B. Gao, F. Li, F. Xu, A colorimetric dermal tattoo biosensor fabricated by microneedle patch for multiplexed detection of health-related biomarkers, Adv. Sci. 8 (24) (2021) 2103030.
[12] E. Xiong, L. Jiang, T. Tian, M. Hu, H. Yue, M. Huang, W. Lin, Y. Jiang, D. Zhu, X. Zhou, Simultaneous dual-gene diagnosis of SARS-CoV-2 based on CRISPR/

Cas9-mediated lateral flow assay, Angew. Chem. Int. Ed. 60 (10) (2021) 5307–5315.
[13] A. Sánchez-Iglesias, N. Claes, D.M. Solís, J.M. Taboada, S. Bals, L.M. Liz-Marzán, M. Grzelczak, Reversible clustering of gold nanoparticles under confinement, Angew Chem. 130 (12) (2018) 3237–3240.
[14] H. Rahimi, M. Salehiabar, M. Barsbay, M. Ghaffarlou, T. Kavetskyy, A. Sharafi, S. Davaran, S.C. Chauhan, H. Danafar, S. Kaboli, CRISPR systems for COVID-19 diagnosis, ACS Sens. 6 (4) (2021) 1430–1445.
[15] J. Shi, F. Tian, J. Lyu, M. Yang, Nanoparticle based fluorescence resonance energy transfer (FRET) for biosensing applications, J. Mater. Chem. B 3 (35) (2015) 6989–7005.
[16] R.M. Clegg, Fluorescence resonance energy transfer, Curr. Opin. Biotechnol. 6 (1) (1995) 103–110.
[17] M. Song, M. Yang, J. Hao, Pathogenic virus detection by optical nanobiosensors, Cell Rep. Phys. Sci. 2 (1) (2021) 100288.
[18] Z. Chen, H. Chen, H. Hu, M. Yu, F. Li, Q. Zhang, Z. Zhou, T. Yi, C. Huang, Versatile synthesis strategy for carboxylic acid– functionalized upconverting nanophosphors as biological labels, J. Am. Chem. Soc. 130 (10) (2008) 3023–3029.
[19] M. Suzuki, Y. Husimi, H. Komatsu, K. Suzuki, K.T. Douglas, Quantum dot FRET biosensors that respond to pH, to proteolytic or nucleolytic cleavage, to DNA synthesis, or to a multiplexing combination, J. Am. Chem. Soc. 130 (17) (2008) 5720–5725.
[20] M. Song, S.Y. Pang, F. Guo, M.C. Wong, J. Hao, Fluoride-free 2D niobium carbide MXenes as stable and biocompatible nanoplatforms for electrochemical biosensors with ultrahigh sensitivity, Adv. Sci. 7 (24) (2020) 2001546.
[21] S.Y. Pang, W.F. Io, L.W. Wong, J. Zhao, J. Hao, Efficient energy conversion and storage based on robust fluoride-free self-assembled 1D niobium carbide in 3D nanowire network, Adv. Sci. 7 (10) (2020) 1903680.
[22] X. Ren, M. Huo, M. Wang, H. Lin, X. Zhang, J. Yin, Y. Chen, H. Chen, Highly catalytic niobium carbide (MXene) promotes hematopoietic recovery after radiation by free radical scavenging, ACS Nano 13 (6) (2019) 6438–6454.
[23] M.K. Tsang, Y.T. Wong, T.H. Tsoi, W.T. Wong, J. Hao, Upconversion luminescence sandwich assay for detection of influenza H7 subtype, Adv. Healthc. Mater. 8 (18) (2019) 1900575.
[24] Z. Yi, Z. Luo, X. Qin, Q. Chen, X. Liu, Lanthanide-activated nanoparticles: a toolbox for bioimaging, therapeutics, and neuromodulation, Acc. Chem. Res. 53 (11) (2020) 2692–2704.